Structure, Vol. 12, 881–891, May, 2004, ©2004 Elsevier Science Ltd. All rights reserved. DOI 10.1016/j.str.2004.02.028

The Focal Adhesion Targeting Domain of Focal Adhesion Kinase Contains a Hinge Region that Modulates Tyrosine 926 Phosphorylation

Kirk C. Prutzman,[1] Guanghua Gao,[1] Michelle L. King,[2] Vidhya V. Iyer,[2] Geoffrey A. Mueller,[6] Michael D. Schaller,[2,3,4,5,*] and Sharon L. Campbell[1,3,*]

[1]Department of Biochemistry and Biophysics
[2]Department of Cell and Developmental Biology
[3]Lineberger Comprehensive Cancer Center
[4]Comprehensive Center for Inflammatory Disorders
[5]Carolina Cardiovascular Biology Center
University of North Carolina at Chapel Hill
Chapel Hill, North Carolina 27599
[6]Laboratory of Structural Biology
National Institute of Environmental Health Sciences
National Institutes of Health
P.O. Box 12233
Research Triangle Park, North Carolina 27709

Summary

The focal adhesion targeting (FAT) domain of focal adhesion kinase (FAK) is critical for recruitment of FAK to focal adhesions and contains tyrosine 926, which, when phosphorylated, binds the SH2 domain of Grb2. Structural studies have shown that the FAT domain is a four-helix bundle that exists as a monomer and a dimer due to domain swapping of helix 1. Here, we report the NMR solution structure of the avian FAT domain, which is similar in overall structure to the X-ray crystal structures of monomeric forms of the FAT domain, except that loop 1 is longer and less structured in solution. Residues in this region undergo temperature-dependent exchange broadening and sample aberrant phi and psi angles, which suggests that this region samples multiple conformations. We have also identified a mutant that dimerizes ~8 fold more than WT FAT domain and exhibits increased phosphorylation of tyrosine 926 both in vitro and in vivo.

Introduction

Focal adhesion kinase (FAK) is a 125 kDa protein that colocalizes with integrins at focal adhesions upon cell adhesion to the extracellular matrix (Parsons, 2003; Schaller, 2001; Schlaepfer et al., 1999). When FAK is recruited to focal adhesions, it becomes activated by a series of phosphorylation events, including autophosphorylation and phosphorylation by Src family tyrosine kinases. Consequently FAK has both catalytic and scaffolding functions in integrin-mediated signaling events. Exogenous overexpression of FAK increases cell motility and promotes cell survival in the absence of extracellular stimuli (Cary et al., 1996; Frisch et al., 1996). Conversely, inhibition of endogenous FAK signaling reduces cell motility and has been shown to induce cell death in some cases (Hungerford et al., 1996; Ilic et al., 1995; Xu et al., 1998). Multiple lines of evidence suggest that FAK may function in the pathology of human cancer, including the observation that FAK is overexpressed in multiple human cancers, including prostate, colon, and breast cancers (Gabarra-Niecko et al., 2003), and is therefore considered to be a potential target for anticancer drug development.

The focal adhesion targeting (FAT) domain located at the carboxy terminus of FAK (residues 920–1040 in avian FAK, 919–1039 in human and murine FAK) is critical for recruitment of FAK to focal adhesions (Hildebrand et al., 1993, 1995). While some studies suggest that the FAT domain recruits FAK to focal adhesions by binding paxillin (Tachibana et al., 1995), other studies indicate that paxillin binding is dispensable for focal adhesion targeting of FAK (Cooley et al., 2000; Hildebrand et al., 1995). Talin has also been proposed as the critical binding partner for the focal adhesion recruitment of FAK (Zheng et al., 1998); however, an analysis of FAK mutants did not reveal a strict correlation between talin binding and localization (Chen et al., 1995). Thus, the mechanism of focal adhesion targeting has not been completely elucidated.

Tyrosine phosphorylation of FAK plays an important role in regulating FAK-mediated signaling (Parsons, 2003; Schaller, 2001; Schlaepfer et al., 1999). One of the sites of FAK phosphorylation is located in the FAT domain at tyrosine Y926 in avian FAK (Y925 in the human and murine FAK sequences). This tyrosine residue exists in a consensus Grb2-SH2 domain binding site (YXNX) and has been shown to bind the SH2 domain of Grb2 when Y925 (in human FAK) is phosphorylated (Schlaepfer et al., 1994). Binding of Grb2 has been shown to facilitate FAK-mediated stimulation of the Ras-MAPK pathway (Schlaepfer and Hunter, 1997). FAK is also able to activate the Ras-MAPK pathway via alternate mechanisms (Schlaepfer and Hunter, 1996), and FAK-independent mechanisms of activating the Ras-MAPK pathway following integrin dependent adhesion have been described (Lin et al., 1997; Wary et al., 1996). Thus, there are multiple mechanisms of regulating MAPK kinase signaling following integrin signaling, only one of which utilizes Y926 phosphorylation of FAK. It is therefore of interest to elucidate additional regulatory mechanisms that may control signaling via this pathway.

Recently, structures of the isolated FAT domain (Arold et al., 2002; Hayashi et al., 2002), as well as the FAT domain liganded to a peptide of paxillin, have been solved (Hoellerer et al., 2003; Liu et al., 2002; Gao et al., 2004). Whereas two of the crystal structures show that the isolated FAT domain adopts a similar antiparallel four-helix bundle (Arold et al., 2002; Hayashi et al., 2002), a third X-ray structure reported a FAT domain dimer due to domain swapping of helix 1 (Arold et al., 2002). FAK has not been demonstrated to dimerize in vivo, and hence, the biological significance of this observation was unclear. Arold et al. (2002) postulated that structural dynamics, particularly in helix 1, might be important

*Correspondence: campbesl@med.unc.edu (S.L.C.), crispy4@med.unc.edu (M.D.S.)

in regulating phosphorylation of Y926 and subsequent binding of the SH2 domain of Grb2. Hence, formation of the domain-swapped dimer at higher concentrations required for crystallization might be a consequence of structural dynamics in helix 1, rather than a functionally relevant dimeric form of the FAT domain. However, as these reports described X-ray crystal structures, structural dynamics were not addressed. Further analyses using alternative methods, e.g., NMR spectroscopy, should aid in elucidating the potential role of FAT domain dynamics in FAK function.

In this study, we report the NMR solution structure of the avian FAT domain. Our results show that the FAT domain is predominantly a monomer in solution and adopts an antiparallel four-helix bundle structure similar to that observed by X-ray crystallography. We have also observed that residues at the carboxy terminus of helix 1, loop 1, and the amino terminus of helix 2 (residues 941–951) display line broadening, suggesting that this region may be subject to conformational exchange in solution. We have designated this region the "hinge region," as it contains a proline-rich motif that may induce strain and promote conformational exchange between an uncharacterized "open" and a "closed" four-helix bundle state. A FAT domain mutant (V955A/L962A) that was previously shown to be defective for paxillin binding was further characterized. We observed by gel filtration that the V955A/L962A mutant exhibits a dramatic shift in the monomer/dimer equilibrium, suggesting that the mutant may favor an open conformation of the FAT domain. This mutant is more readily phosphorylated by Src in vitro and shows increased phosphorylation at Y926 in vivo, compared to WT FAK. Although other possible roles of hinge dynamics may exist, our results are consistent with the hypothesis that structural dynamics of the FAT domain may play an important role in determining Y926 phosphorylation and linkage of FAK to the Ras-MAPK kinase signaling pathway.

Results

The FAT domain adopts a monomeric, amphipathic four-helix bundle in solution (see Table 1 for structure statistics), similar to that observed in two of the three reported X-ray crystal structures (Figures 1A and 1B). The 12 amino acid linker at the amino terminus remaining from purification is not structured in solution and does not have any contacts with the FAT domain; therefore, we consider it to be inconsequential to the final structure. The most significant difference between the X-ray crystal structures of the monomeric form of the FAT domain and the family of NMR solution structures is in the region we have defined as the hinge region (residues 941–951) (Figures 1B and 1C). Both monomeric X-ray crystal structures suggest that helix 1 extends to I943 (Arold et al., 2002) or Q944 (Hayashi et al., 2002) and helix 2 starts at P947. Between the two helices is a short loop. In contrast, the NMR solution structures indicate that this region is not structured, since helix 1 ends at S940 and helix 2 begins at V952, and the intervening sequence forms an extended loop between residues S941 and Y951. Careful analysis of the NOE distance restraints in the hinge region against predicted restraints (from the X-ray crystal structures) demonstrated that this is a less structured region in solution.

Table 1. Summary of Structural Statistics

NOEs[a]	
H-CH	1612
H-NH	1093
Unambiguous	1627
Ambiguous	1078
Total	2705
Ensemble rmsd (Å)	
Secondary structure (backbone)[a]	0.31 ± .031
Secondary structure (heavy)[a]	0.76 ± .075
Backbone (residues 920–1053)[b]	1.69 ± 0.40
Heavy (residues 920–1053)[b]	2.51 ± 0.41
Backbone (residues 927–1047)[b]	1.00 ± 0.16
Heavy (residues 927–1047)[b]	1.74 ± 0.18
Violations (experimental restraints)[a]	
NOEs and H bonds	5.43
Dihedral angles	2.71
Rmsd (experimental restraints)[a]	
NOEs (Å)	0.105 ± 0.042
H Bonds (Å)	0.403 ± 0.010
Dihedral angles (°)	2.15 ± 0.93
Residual dipolar coupling (Hz)	1.175 ± 0.040
Rmsd (covalent geometry)[a]	
Bonds (Å)	0.0052 ± 0.0002
Angles (°)	0.927 ± 0.0166
Impropers	2.50 ± 0.0970
Ramachandran space[c]	
Most favored (%)	90
Additionally allowed (%)	7
Generously allowed (%)	2.1
Dissallowed (%)	0.9

[a] Output by ARIA (Nilges, 1995), calculated by CNS (Brunger et al., 1998) using the ensemble of the 20 lowest energy structures.
[b] Calculated with the program MOLMOL (Koradi et al., 1996).
[c] Calculated with PROCHECK (Laskowski et al., 1996).

Temperature-Dependent Detection of Amide Resonances Associated with the Hinge Region

In addition to the longer, unstructured loop 1, many (^{1}H-^{15}N)-HSQC peaks were either lost or significantly broadened when NMR experiments were performed at 27°C rather than 37°C (Figure 2A). When the temperature-dependent resonances are mapped to residues on the three-dimensional structure of the FAT domain, many of these residues are colocalized in and around the hinge region (Figure 2B). The ability to detect resonances in the hinge region at 37°C but not at 27°C suggests that resonances associated with the hinge region may be in intermediate exchange on the NMR time scale at 27°C and at fast-intermediate exchange at 37°C. Interestingly, additional amide resonances that exhibited exchange-broadening characteristics are either located in loop 3 (opposite to the hinge region) or correspond to hydrophobic residues involved in hydrophobic core contacts between helices. (^{1}H-^{15}N)-HSQC spectra collected at 800 MHz show reduced relative intensity in the amide resonances associated with residues in and around the hinge region relative to spectra collected at 600 MHz (data not shown), providing further support for conformational exchange of residues in the region of the hinge.

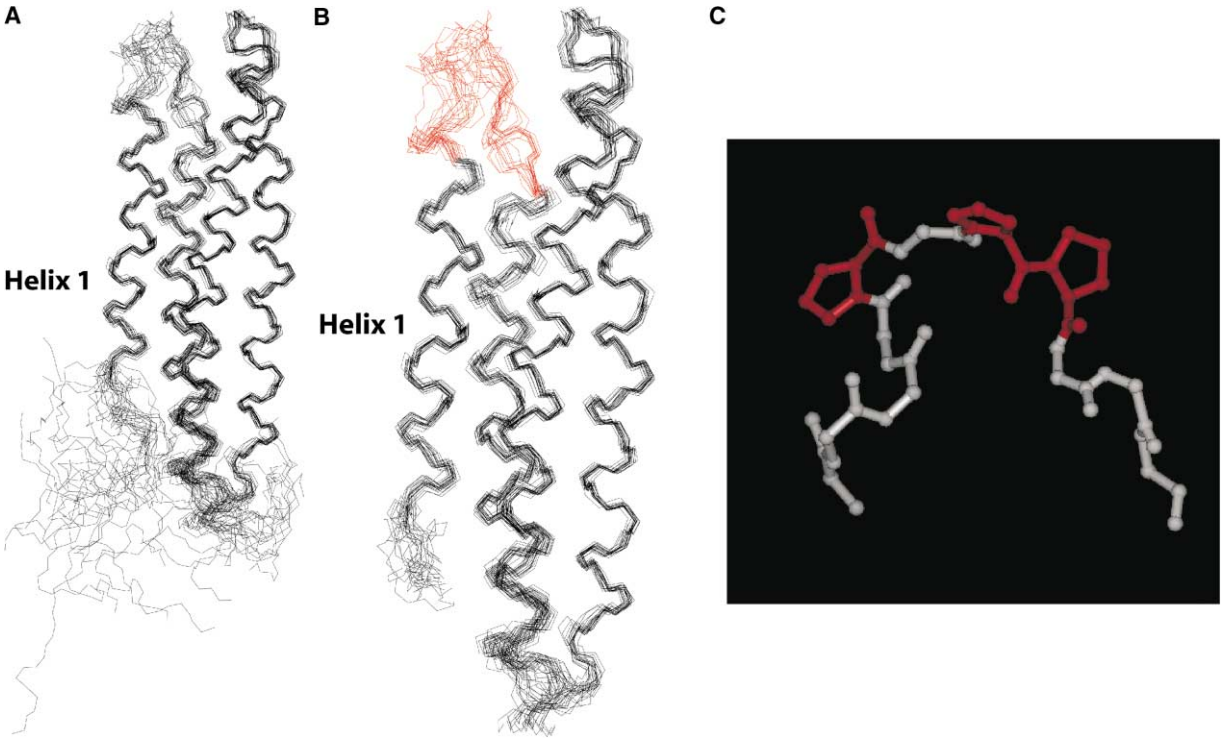

Figure 1. Solution Structure of the Avian FAT Domain

(A) Backbone atom trace of the 20 lowest energy solution structures of the avian FAT domain (residues 920–1053), with a 12 amino acid linker at the amino terminus remaining from purification.

(B) The backbone trace of the avian FAT domain minus the 12 amino acid linker. The proposed hinge region (residues 941–951) is colored red.

(C) Expanded view of the hinge region, which contains three prolines (P945, P947, and P948, in red).

Residues in the Hinge Region Exhibit Anomalous Phi and Psi Angles

A structural analysis of the 20 reported solution structures using the program PROCHECK (Laskowski et al., 1996) revealed that residues in the hinge region (residues 943–951) sample aberrant phi and psi angles as determined by low average G factor values. The G factor provides a measure of how "normal" or alternatively how "unusual" a given stereochemical property is, with a low G factor indicating that the property (phi/psi torsion angle in this case) corresponds to a low probability conformation. Consistent with our premise that the proline-rich region may be a source of conformational strain, low G factors are observed for two or more residues in the hinge region in each structure of the ensemble. The only other region of the FAT domain that has a significant number of residues with low average G factor values is loop 2 (residues 973, 975–978), which contains proline residues at 974 and 977 (residues 973 and 976 in the human FAT domain) that may be responsible for the aberrant phi-psi angles. A PROCHECK structural analysis of the 20 avian FAT domain solution structures also showed that the same residues have high circular variance values. The circular variance provides a measure of the spread of a set of dihedral angles and is a measure of how tightly or loosely a given residue's phi or psi torsion angles cluster together across the entire family or ensemble. Similar phi and psi angle violations in hinge residues 946–950 (corresponding to residues 947–951 in the avian FAT domain) were observed in the X-ray crystal structure of the mouse FAT domain reported by Hayashi et al. (2002). In addition, the monomeric form of the human FAT domain reported by Arold et al. (2002) showed low G factor values for residues 939–950 (residues 940–951 in the avian FAT domain). In this study, the monomer crystallized with three molecules in the unit cell. Interestingly, there was variability in the G factor values of the residues in the hinge region among the three molecules, suggesting that this region adopts multiple conformations. In contrast, only a slight phi-psi angle violation was observed in P944 (945 in the avian FAT domain) in the structure of the domain-swapped dimer (Arold et al., 2002). The observed phi-psi angle violations, high circular variance, and temperature-dependent amide peak broadening in the hinge region of the FAT domain suggest conformational strain in this region. Conformational strain in the hinge region may be reduced in the domain-swapped dimer.

Conformation of the FAT Domain May Regulate Y926 Phosphorylation

Analysis of previous structural data indicates that the consensus, YXNX, Grb2 binding sequence must adopt a conformation(s) distinct from its conformation in helix 1 (Figure 3A) to be phosphorylated (Hubbard, 1997) and bind Grb2 (Rahuel et al., 1996). It has been previously

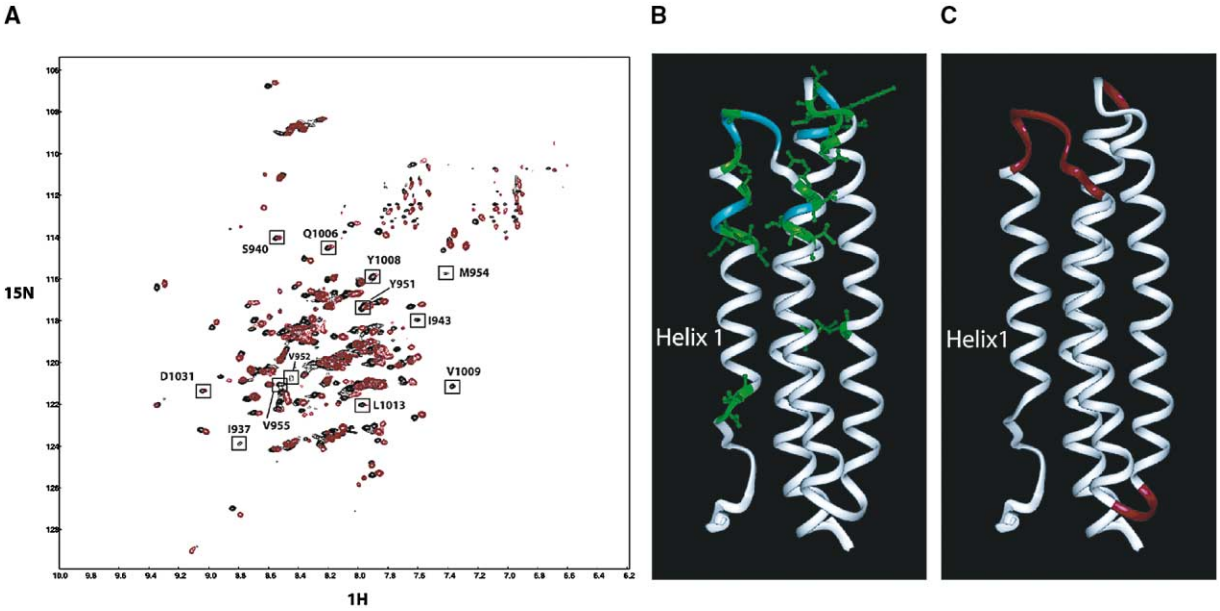

Figure 2. Exchange Broadened Residues and Residues with Phi-Psi Violations

(A) Overlay of (^{1}H-^{15}N)-HSQC spectra collected at 37°C (black) and 27°C (red). Resides that show temperature-dependent exchange broadening are indicated with a box and labeled. Residues A946, V936, and T1011 also exhibit exchange broadening but are not shown because they are observed only at lower contour levels.

(B) Backbone H-N peaks in the (^{1}H-^{15}N)-HSQC spectra that are either unobservable or significantly less intense when the temperature is lowered from 37°C to 27°C (in green). The blue/gray residues depict resonances associated with residues for which exchange broadening cannot be assessed, due to either spectral overlap, lack of signal, or the presence of a proline residue lacking a backbone H-N peak.

(C) Residues that have aberrant phi-psi angles (red ribbon) as determined by low average G factor values using the program PROCHECK (Laskowski et al., 1996).

suggested that conformational flexibility within the FAT domain may promote an "open" conformation of helix 1 required for phosphorylation at Y926 (Arold et al., 2002). Hydrogen exchange experiments on the FAT domain conducted in this lab (data not shown) and by others (Hoellerer et al., 2003) show that residues in helix 1 exchange faster than residues in α helices 2–4, providing evidence that helix 1 is less protected from solvent exchange relative to other structural elements in the FAT domain. To further explore the role of FAT domain hinge dynamics, in particular conformational dynamics associated with helix 1 in modulating phosphorylation of Y926, the phosphorylation of recombinant fusion proteins derived from the FAT domain was examined in vitro. To mimic an open conformation, the sequence encoding helix 1 was expressed as a GST fusion protein. Phosphorylation of this substrate by an activated Src variant (Src^{527F}) was compared to phosphorylation of a GST-FAT domain fusion protein (Figure 3B). Samples were analyzed by SDS-PAGE and phosphorimager analysis. GST alone was modestly phosphorylated by Src in vitro. The GST-helix 1 fusion protein was phosphorylated approximately 8-fold more than the GST-FAT domain. These results demonstrate that the sequence encoding helix 1 is a better Src phosphorylation substrate than the intact FAT domain, consistent with the hypothesis that regulation of the FAT domain conformation could play an important role in regulating Y926 phosphorylation and signaling via the MAP kinase pathway.

V955A/L962A Exhibits Increased Y926 Phosphorylation

The previously reported V955A/L962A FAT domain mutant possesses an interesting property in that it failed to bind paxillin while retaining the ability to target FAK to focal adhesions (Cooley et al., 2000). Both V955 and L962 are located in helix 2 of the FAT domain and are partially buried in the helix 2-helix 3 interface, with V955 proximal to the hinge region (Figure 4A). Mutation of partially buried residues associated with the helix bundle core could increase the tendency of the V955A/L962A FAT domain mutant to dimerize due to disruption of helix packing interactions. Thus, the level of dimerization of the WT FAT domain and the V955A/L962A mutant were compared by gel filtration. Figures 4B and 4C show the elution profiles of 0.5 mM WT FAT domain and V955A/L962A FAT domain eluted over an S-75 gel filtration column. Integration of the monomer and dimer peaks shows that the V955A/L962A mutant dimerizes at a level approximately eight times greater than WT-FAT domain.

As the V955A/L962A mutant exhibited increased propensity to dimerize, it was examined to determine if it might serve as a better substrate for Src than the WT FAT domain. Src-mediated tyrosine phosphorylation of the mutant and WT FAT domains, expressed as GST fusion proteins, in an in vitro immune complex kinase assay revealed a 1.8-fold increase in tyrosine phosphorylation of the mutant relative to WT protein (Figure 5).

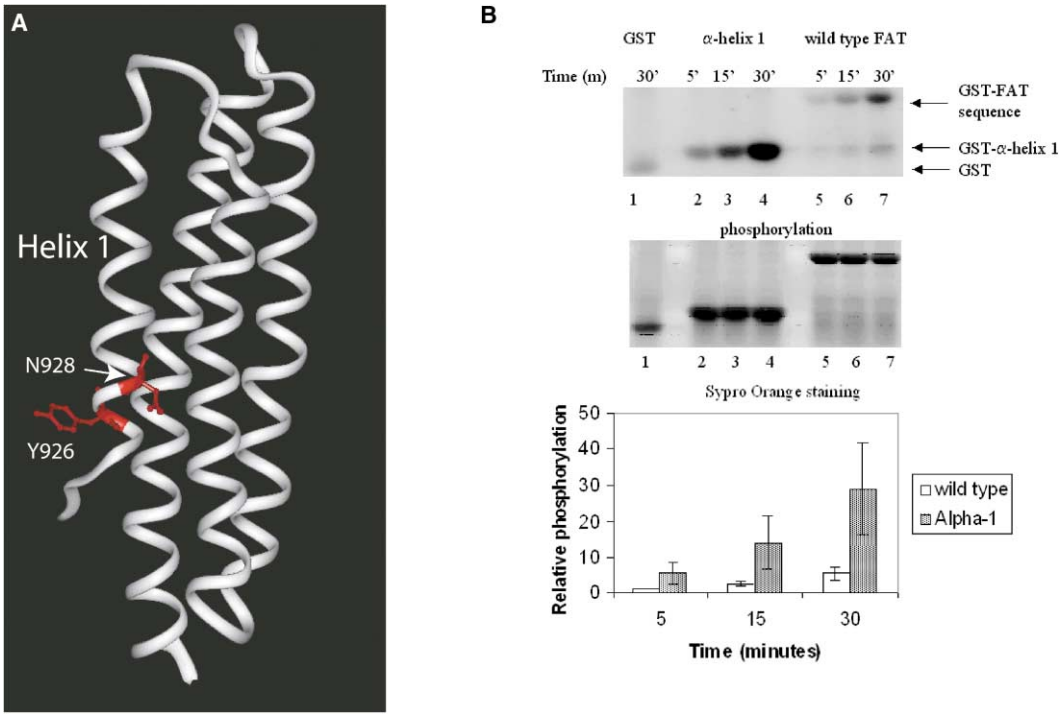

Figure 3. Tyrosine Phosphorylation of Helix 1 In Vitro

(A) The Grb2-SH2 binding site (YXNX) located in helix 1 of the FAT domain (YENV). Y926 and N928 are colored in red.

(B) Src^{527F} immune complexes were incubated in in vitro kinase assays containing GST (lane 1), GST-helix 1 (lanes 2–4), or GST-FAT sequence (lanes 5–7) as exogenous substrate. Reactions were terminated at the indicated time, and the samples were analyzed by SDS-PAGE. Incorporation of ^{32}P into substrates was quantified by phosphorimager analysis (top panel), and the amount of substrate was quantified by Sypro orange staining and visualization using the Storm phosphorimager (middle panel). A representative experiment is shown in the top panels. Quantification of multiple experiments ($n = 5$) is shown in the histogram at the bottom. Phosphorylation was normalized for the amount of substrate in the reaction. The level of phosphorylation of the GST-FAT domain substrate after 5 min was set at a relative phosphorylation of 1.

These results demonstrate that the V955A/L962A mutant serves as a moderately better substrate than the WT FAT domain in the in vitro kinase assay.

To explore tyrosine phosphorylation of V955A/L962A in vivo, WT FAK, epitope-tagged FAK, and epitope-tagged V955A/L962A were expressed in CE cells using the RCAS A retroviral vector. Cells were lysed, and phosphorylation of Y926 was examined by Western blotting lysates with the PY925 antibody. Consistent with previous studies (Gabarra-Niecko et al., 2002; Thomas et al., 1998), neither endogenous FAK nor exogenously expressed WT FAK exhibited detectable tyrosine phosphorylation at residue 926 (Figure 6A, top panel). The epitope-tagged FAK exhibited a very slight increase in phosphorylation of tyrosine Y926. In contrast, V955A/L962A exhibited a dramatic increase in the level of tyrosine Y926 phosphorylation. The blot was stripped and reprobed with the BC4 FAK polyclonal antiserum to demonstrate comparable levels of protein (Figure 6A, bottom panel). A previous study revealed that coexpression of FAK with c-Src resulted in increased association of FAK with the Grb2 SH2 domain in vitro (Thomas et al., 1998). This result was interpreted as an increase in the level of tyrosine Y926 phosphorylation upon coexpression with Src. To validate this conclusion, c-Src was coexpressed with WT FAK, and phosphorylation was examined by blotting with PY925 (Figure 6B, top panel). Indeed, coexpression with c-Src dramatically increased the level of phosphorylation of tyrosine Y926. Coexpression of c-Src with epitope-tagged FAK produced a higher level of 926 phosphorylation than WT FAK. Further, expression of c-Src with V955A/L962A resulted in an even higher level of phosphorylation at tyrosine Y926. The blot was stripped and reprobed with BC4 to demonstrate comparable FAK protein levels in each sample (Figure 6B, middle panel). These results demonstrate that one consequence of the V955A/L962A mutation is an increase in the level of tyrosine 926 phosphorylation both in vitro and in vivo.

Discussion

Although the overall solution structure of the avian FAT domain (residues 920–1053 of FAK) is in agreement with X-ray structures of monomeric forms of the FAT domain (Arold et al., 2002; Hayashi et al., 2002), loop 1 is longer and less structured in solution. Loop 1 is a proline-rich region that links helix 1 and helix 2. We propose that loop 1 serves as a "hinge" region that induces conformational strain in the FAT domain to perturb packing interactions, thereby promoting conformational exchange between a closed helix bundle and a more open conformation. The open conformation promotes phosphorylation of Y926,

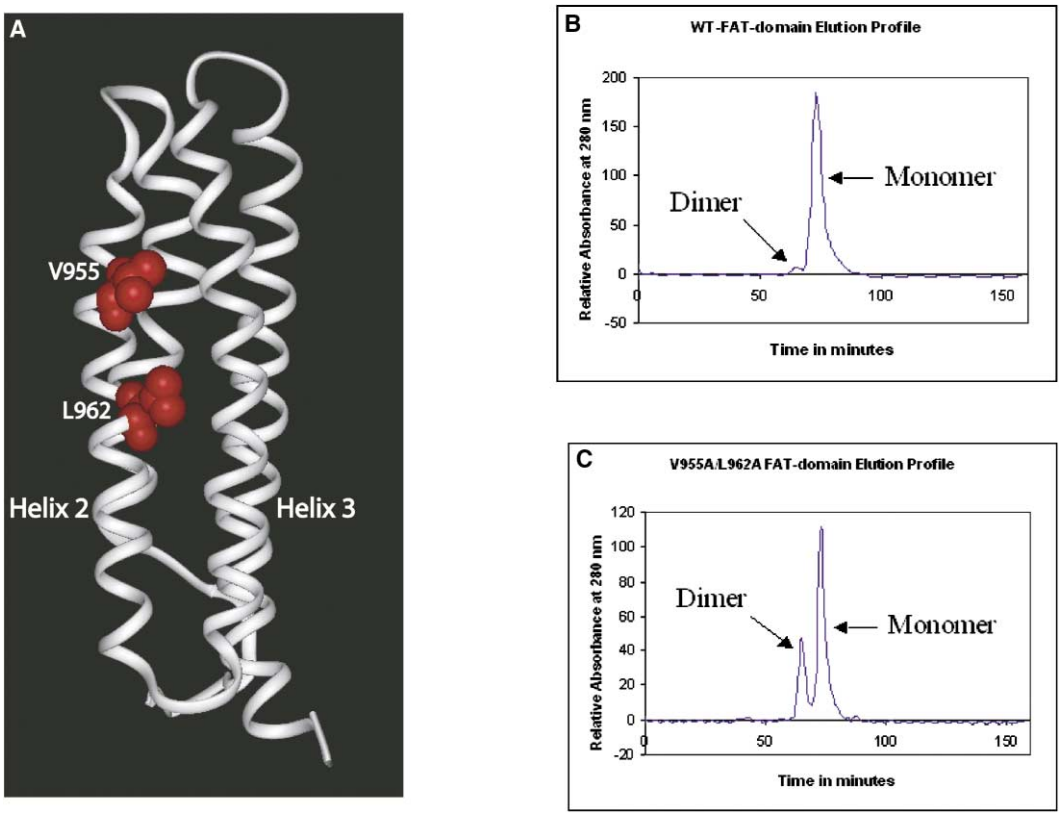

Figure 4. Sephadex-75 Gel Filtration Elution Profiles of WT FAT and the V955A/L962A FAT Domain

(A) Residues V955 and L962 (in red) are mapped and labeled on the structure of the FAT domain. (B) 0.5 mM WT-FAT domain or (C) V955A/L962A FAT domain was eluted over a Sephadex-75 gel filtration column at a flow rate of 0.3 ml/min. The monomer and dimer peaks are labeled. Integration of the peaks and analysis (see Experimental Procedures) show the dimeric form of the FAT domain is populated at ~8-fold higher levels in the V955A/L962A mutant relative to the WT FAT domain.

self-association in vitro, and formation of a domain-swapped dimer under conditions of crystallization.

Role of the Hinge Region in FAT Domain Conformational Dynamics

These structural studies provide potential insight into the mechanism of localized conformational dynamics in the FAT domain. The three prolines in the hinge region may create conformational strain due to reduced intrinsic conformational flexibility and thus may sample multiple conformations, an interpretation consistent with the observed amide resonance exchange broadening in and around the hinge region detected by NMR. Monomer-dimer equilibrium may result from competition between favorable hydrophobic helix packing and unfavorable strain in the hinge region.

In this regard, the hinge region of the FAT domain may resemble the "switch region" of the cyclin-dependent kinase subunit, $p13^{suc1}$ (Odaert et al., 2002; Rousseau et al., 2001). Domain swapping of β strand 4 between two molecules of $p13^{suc1}$ results in homodimerization (Rousseau et al., 2001). NMR structural analysis of $p13^{suc1}$ revealed phi-psi angle violations (Rousseau et al., 2001) and exchange broadening (Odaert et al., 2002) within the proline-rich switch region. It was postulated that the proline residues in the $p13^{suc1}$ hinge region create conformational strain that is relieved in the domain-swapped dimer (Rousseau et al., 2001). Mutating residues in the "switch region" of $p13^{suc1}$ to create more strain (i.e., adding more prolines or removing nonproline residues) resulted in increased dimerization while relieving strain (i.e., mutating prolines to alanines) resulted in decreased dimerization.

Potential Biological Significance of FAT Domain Conformational Exchange

Although the biological relevance of conformational dynamics, induced by the hinge region, is not clear at this point in time, one potential role may be FAT domain homodimerization. The exchange broadening observed by NMR for resonances in the hinge region may result in helix 1 sampling "open" conformations, thereby exposing the hydrophobic core, promoting domain swapping as observed in the X-ray crystal structure. Since there is no evidence of FAT domain dimerization in vivo, it is possible that the domain-swapped dimer is formed only at high concentrations necessary for X-ray crystallography. The most likely function of hinge dynamics is regulation of phosphorylation and/or ligand binding. Structural data suggests that paxillin binds the FAT domain in a rigid four-helix bundle conformation and does not require any significant structural changes

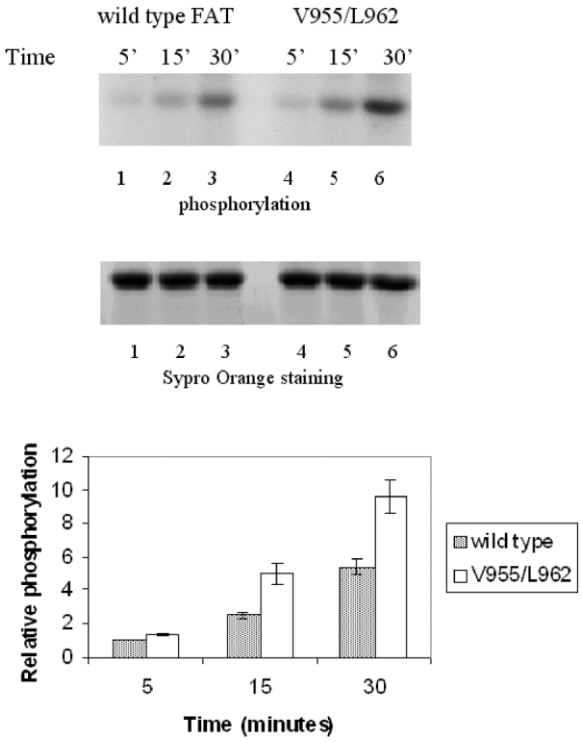

Figure 5. Tyrosine Phosphorylation of V955A/L962A In Vitro

Src^{527F} immune complexes were incubated in in vitro kinase assays containing GST-WT FAT domain (lanes 1–3) or GST-V955A/L962A FAT domain (lanes 4–6) as exogenous substrate. Reactions were terminated at the indicated time, and the samples were analyzed as in Figure 3. A representative experiment is shown in the top panels. Quantification of multiple experiments (n = 5) was performed as in Figure 3 and is shown in the histogram at the bottom.

(Gao et al., 2004; Hoellerer et al., 2003; Liu et al., 2002). In the case of paxillin binding, conformational mobility may function to reduce binding. However, binding of the SH2-domain of Grb2 to the FAT domain may require a conformational change. In this case, hinge dynamics may be required to promote Grb2 binding.

The conformation of residues comprising the Grb2 consensus sequence within helix 1 of the FAT domain appears to impose a structural constraint upon tyrosine phosphorylation and Grb2 binding (Arold et al., 2002; Hoellerer et al., 2003). In order to achieve phosphorylation and subsequent Grb2-SH2 domain binding, it appears that Y926 and surrounding residues must undergo structural rearrangement (Hubbard, 1997; Rahuel et al., 1996). It is possible that the conformational dynamics in the hinge region promotes the conformational freedom of helix 1 necessary for phosphorylation and Grb2 binding. Our results show that the sequence corresponding to helix 1 is a better substrate than the intact FAT domain for Src-mediated tyrosine phosphorylation in vitro, consistent with the premise that structural flexibility of helix 1 is required to allow Y926 and the surrounding amino acids to adopt a more linear conformation resulting in higher levels of Y926 phosphorylation.

The V955A/L962A Mutant

The V955A/L962A mutant has alanine substitutions in place of two hydrophobic residues that are partially buried in the FAT domain. This mutant exhibits a loss of paxillin binding. Since paxillin binds to two sites on opposite faces of the FAT domain (Gao et al., 2004; Hayashi et al., 2002; Hoellerer et al., 2003), this mutant presumably alters the conformation of the FAT domain to disrupt both binding sites. While it is possible that the mutations simply disrupt the structure of the FAT domain, several lines of investigation suggest that this is not the case.

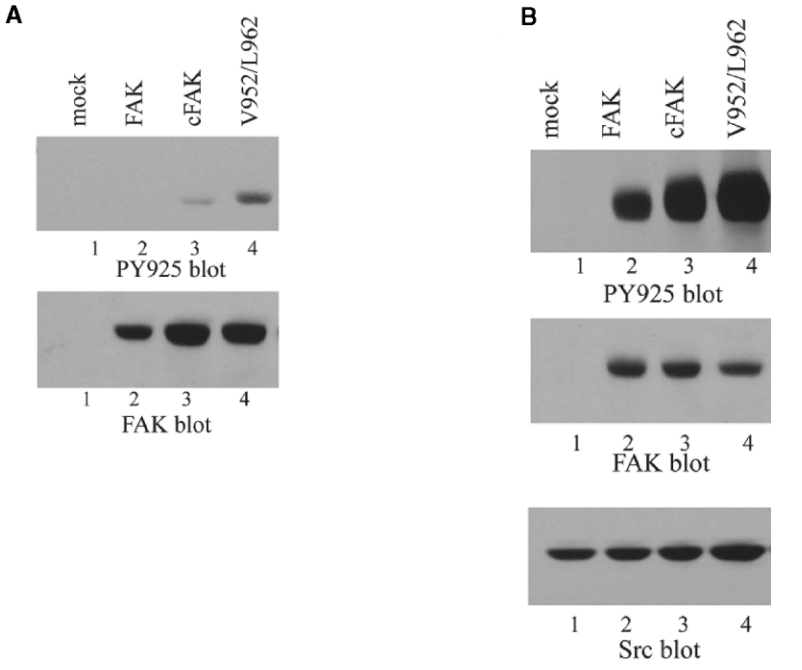

Figure 6. Tyrosine Phosphorylation of Tyrosine 926 In Vivo

Lysates from control CE cells (lanes 1) and cells overexpressing WT FAK (lanes 2), C-terminally epitope-tagged FAK (lanes 3), or C-terminally epitope-tagged V955A/L962A (lane 4) were analyzed by Western blotting using the PY925 phospho-specific antibody (top panels) or a FAK polyclonal antibody. Cells expressing FAK alone (A) or coexpressing FAK and c-Src (B) were analyzed. A Src blot to verify expression of c-Src is shown in the bottom panel of (B).

First, circular dichroism spectra of WT and mutant FAT domain sequences are identical (data not shown). Second, the mutant is recognized by monoclonal antibody 2A7, which is believed to be a conformation-specific antibody (Cooley et al., 2000). Third, the mutant can correctly localize to focal adhesions when expressed in CE cells (Cooley et al., 2000).

Our results show that the V955A/L962A variant dimerizes ~8-fold more than the WT FAT domain and exhibits a higher level of phosphorylation relative to the WT FAT domain both in vitro and in vivo. Enhanced dimerization and Y925 phosphorylation associated with this mutant may be due to disruption of packing interactions within the four-helix bundle, which may, in turn, populate "open" conformations associated with helix 1. While additional analyses are required to determine the precise conformations adopted by the V955A/L962A mutant, the increased phosphorylation of Y926 in the mutant supports the concept that alteration of FAT domain conformations may modulate downstream signaling.

The V955A/L962A double mutant may provide insight into other aspects of FAK biology. The V955A/L962A mutant was of interest originally because it was recruited to focal adhesions but was deficient in paxillin binding. As one paxillin binding site lies on the helix 1-helix 4 face, association with paxillin may inhibit Y926 phosphorylation and subsequent Grb2 binding. Thus, FAT domain dynamics and paxillin binding may play antagonistic roles in regulating phosphorylation of Y926 and Grb2 binding. As Grb2 binding to FAK is one mechanism linking FAK to regulation of the Ras-MAPK signaling pathway (Schlaepfer et al., 1994), paxillin binding may regulate downstream Ras signaling events. Further, distinct populations of FAK may elicit distinct downstream signals; e.g., paxillin-free FAK, but not paxillin-bound FAK, may engage Grb2 and subsequently activate Ras and MAPK signaling. In a recent study, it was speculated that Y925 phosphorylation and Grb2 binding might interfere with binding to paxillin and talin, resulting in the loss of FAK from focal adhesions (Katz et al., 2003). Thus, it is possible that conformational plasticity in the FAT domain may also control the subcellular localization of FAK by regulating phosphorylation and ligand binding. While some of these recent findings are very provocative, further analysis of the FAT domain dynamics by NMR and analysis of mutants with altered dynamics will be required to fully elucidate the role of FAT domain dynamics in FAK function.

Experimental Procedures

Molecular Biology

The construct expressing the GST-WT FAT domain fusion protein has been described (Thomas et al., 1999). A similar PCR-based strategy was used to engineer the GST fusion protein containing the V955A/L962A mutant FAT sequence (Cooley et al., 2000). A PCR-based strategy was also used to create the vector encoding helix 1 of the FAT domain fused in-frame with GST. A termination codon was engineered in place of P947 in this construct. The nucleotide sequence of each of the subcloned, amplified sequences was determined at the UNC-CH Automated DNA Sequencing Facility.

Expression and Purification of the FAT Domain of FAK

The FAT domain, containing residues 920–1053 of avian FAK plus a 12 amino acid N-terminal linker (sequence: GSPGISGGGGGIRSND KVYENVTGLVKAVIEMSSKIQPAPPEEYVPMVKEVGLALRTLLATVDE SLPVLPASTHREIEMAQKLLNSDLAELINKMKLAQQYVMTSLQQEYK KQMLTAAHALAVDAKNLLDVIDQARLKMISQSRPH), was expressed as a GST fusion protein as previously described (Thomas et al., 1999). Bacteria were grown at 37°C in a minimal media containing ^{15}N-NH_4Cl (1 g/liter) (Isotec) and ^{13}C-D-glucose (3 g/liter) (Isotec). The FAT fusion protein was purified on glutathione agarose beads. The FAT domain was cleaved from the GSH agarose beads by incubation with thrombin (0.4 U/mg of protein) and purified further by chromatography on a mono S column. Residual thrombin was inhibited by the addition of PPACK (1 μM) and pefabloc (0.5 mg/ml). The lysine (−) and ^{15}N-leu samples were grown and expressed in a minimal media enriched with specific amino acids as previously described (McIntosh and Dahlquist, 1990). Specifically isotopically enriched proteins were purified as described above.

NMR Samples

Purified proteins were exchanged into NMR buffer (25 mM Tris-d_{11} Maleate-d_2 [pH 6.0], 150 mM NaCl, 0.1% NaN_3, PPACK [1 μM], pefabloc [0.5 mg/ml], and 10% D_2O) using a Centricon (MW cutoff, 5000). The FAT domain was concentrated to 0.85 mM and transferred to a Wilmad NMR tube.

NMR Spectroscopy

A simultaneous 3D $^{13}C/^{15}N$-NOESY (Grzesiek and Bax, 1992; Pascal et al., 1994) three-dimensional data set was collected on a Varian INOVA 800 MHz spectrometer at 37°C. All other data were collected on a Varian INOVA 600 MHz spectrometer at 37°C. NMR spectra were processed with NMRPipe (Delaglio et al., 1995) and analyzed with NMRView (Johnson and Blevins, 1994). Backbone sequential assignments were determined manually from the following series of multidimensional triple-resonance experiments on a sample of uniformly $^{13}C/^{15}N$-enriched FAT domain: (^1H-^{15}N)-HSQC (Kay et al., 1992), HNCA (Ikura et al., 1990), HNCOCA (Matsuo et al., 1996), HNCACB (Wittekind and Mueller, 1993), CBCA(CO)NH (Grzesiek and Bax, 1992), HNCO (Kay et al., 1994), $^{13}C/^{15}N$-edited NOESY, and (H)C(CO)-TOCSY-NH (Grzesiek et al., 1993). (^1H-^{15}N)-HSQC spectra were also collected on specifically enriched ^{15}N-lysine (−) and ^{15}N-leucine samples to verify assignments. Side chain assignments were determined from the following experiments: HNCACB, CBCA(CO)NH, HCCH-COSY (Ikura et al., 1991), H(CCO)-TOCSY-NH (Grzesiek et al., 1993), and (H)C(CO)-TOCSY-NH. Aromatic side chain assignments were obtained from HBCB(CGCDCE)HE (Yamazaki et al., 1993) and HBCB(CGCD)HD (Yamazaki et al., 1993) experiments. All spectra were referenced directly (^1H) and indirectly (^{13}C and ^{15}N) to DSS.

Residual Dipolar Coupling Measurements

Pf1 phage (ASLA Ltd.) was exchanged into NMR buffer by centrifugation and added to a 0.25 mM sample of $^{13}C/^{15}N$-labeled FAT domain at a final concentration of 7.5 mg/ml. To insure that the FAT domain did not bind phage, (^1H-^{15}N)-HSQC spectra were collected on 0.25 mM FAT domain in 7.5 mg/ml NMR buffer + pf1-phage as well as 0.25 mM FAT domain in NMR buffer alone. No significant differences were observed in the (^1H-^{15}N)-HSQC spectra of the FAT domain in NMR buffer + phage. (^1H-^{15}N)-HSQC-IPAP (Ottiger et al., 1998) and HNCOCAHA-IPAP (Yang et al., 1998) spectra were collected on both FAT domain in NMR buffer + phage and FAT domain in NMR buffer to measure the $^1H^N$-^{15}N and $^1H^\alpha$-$^{13}C^\alpha$ residual dipolar couplings, respectively. Spectra were collected to a resolution of 17.2 Hz/Pt (linear predicted to 8.6 Hz/Pt.) and 22.5 Hz/Pt (linear predicted to 11.1 Hz/Pt) in the ^{15}N dimension of the (^1H-^{15}N)-HSQC-IPAP spectrum and the indirect ^1H dimension of the HNCOCAHA-IPAP spectrum, respectively. Coupling differences of −16.4 Hz to 4.4 Hz were observed in the (^1H-^{15}N)-HSQC-IPAP spectrum and −11.4 Hz to 22.9 Hz in the HNCOCAHA-IPAP spectrum. Residual dipolar coupling constants were fit to preliminary FAT domain structures, and a rhombicity value was generated using the program RDCA (Yang et al., 1999). Residues in loop regions were discarded. Sixty-nine $^1H^N$-^{15}N and 95 $^1H^\alpha$-$^{13}C^\alpha$ residual dipolar coupling constants were used for structure calculations.

Structure Calculations

NOE distance restraints, hydrogen bonds, and dihedral angles, in addition to $^{1}H^{N}$-^{15}N and $^{1}H^{\alpha}$-$^{13}C^{\alpha}$ residual dipolar coupling restraints, were used in structure calculations of the FAT domain using the crystal structure from Hayashi et al. (2002) as a starting template. The program Insight II (Accelrys, San Diego, CA) was used to engineer the 12 amino acid linker onto the amino terminus and introduce amino acid substitutions (T972S, I973L, A975V, G996A, S1000N, L1046I, G1047S, and T1049S) into the Hayashi et al. (2002) crystal structure (1K40) to model the starting construct used in this study. Dihedral angle restraints were derived from the Cα chemical shifts using the program TALOS (Cornilescu et al., 1999). Calculated dihedral angle restraints for residues corresponding to loop regions in the three-dimensional structure were discarded from structure calculations. The remaining calculated dihedral angle restraints were used in structure calculations only if the dihedral angle was a "good" match as established by TALOS criterion. Errors were set at ±2 times the standard deviation or at least ±20°. Hydrogen bond restraints were determined from the TALOS-predicted secondary structure as well as the crystal structure (1K40). H bond (97) and dihedral angle (83) restraints were also used in structure calculations. The residual dipolar coupling values were globally fit to the engineered FAT domain crystal structure from Hayashi et al. (2002), and a rhombicity value of 0.5075 was obtained. Uncertainties were estimated at 1.5 Hz for $^{1}D_{NH}$ and 2.0 Hz for $^{1}D_{C\alpha H\alpha}$.

The program CNS (version 1.1) (Brunger et al., 1998) using the module ARIA (version 1.2) (Linge and Nilges, 1999; Nilges, 1995, 1997) was employed for structure calculations of the avian FAT domain. The structural restraints included the H bond, dihedral angle, and the RDC restraints as described above. The NOE distance restraints were derived from $^{13}C/^{15}N$-NOESY peak lists. The peak lists were constructed by the NMRView program and edited manually to remove any water and apodization artifacts. Thirteen long-range, interhelix NOE cross peaks were assigned manually, and the remaining peaks in the peak list were left unassigned. All peaks in the peak lists were uncalibrated. NOE cross-peaks assigned by Aria were inspected manually to verify assignments.

The engineered FAT domain was used as an initial starting structure and a template for automated NOE assignments in the first iteration of Aria-CNS structure calculations. The following set of parameters produced the best convergence: ρ = (0.95, 0.95, 0.95, 0.94, 0.93, 0.92, 0.91, 0.90, 0.80), violtoler = (5.0, 2.0, 1.0, 0.5, 0.25, 1.0, 0.1, 0.1, 0.1), and a maxn = 5 for all iterations. The rotational correlation time (τ_c) was estimated to be 9.5 ns (compared with proteins of similar size) and was used in the calibration of NOE distances in the ARIA structure calculations. The 20 lowest energy structures of the avian FAT domain have been submitted to the PDB under code number 1PV3.

Gel Filtration Measurements

Purified FAT domain and the V955A/L962A FAT domain variant were concentrated to 0.5 mM and resolved by Sephadex 75 gel filtration on an Amersham-Pharmacia Biotech ÄKTA-FPLC. All samples were eluted over the column at 0.3 ml/minute in elution buffer (25 mM Tris-Maleate [pH 6.0], 150 mM NaCl, 0.1% NaN_3). The elution profiles were examined and the peaks were integrated using Unicorn 3.10 software. Elution profiles were compared with known molecular weight standard elution profiles. The eluted peaks were collected and analyzed by SDS-PAGE. Monomer-dimer equilibrium constants were calculated from the following equations:

$$2\ \text{Monomer} \rightleftharpoons \text{Dimer} \quad (1)$$

$$\%\text{Dimer} = [\text{Dimer}]/([\text{Dimer}] + 2[\text{Monomer}]) \quad (2)$$

$$\%\text{Dimer}_{\text{ratio}} = \%\text{Dimer}_{mut}/\%\text{Dimer}_{wt} \quad (3)$$

To ensure that the monomer was in equilibrium with the dimer, fractions that contained monomer or dimer FAT domain were combined separately, concentrated to 0.5 mM, separated by Sephacryl-75 gel filtration, and analyzed as discussed above. These results were also confirmed from multiple preparations of WT FAT domain and the V955A/L962A mutant.

Cells and Viruses

Primary chicken embryo (CE) cells were prepared and maintained as previously described (Reynolds et al., 1989). Exogenous FAK and Src were expressed using the RCAS A and RCAS B replication-competent avian retroviral vectors. RCAS A containing cDNAs encoding WT FAK, epitope-tagged FAK and $FAK^{V955A/L962A}$, the RCAS B/c-Src construct, and $pRLSrc^{527F}$ have been described (Cooley et al., 2000; Reynolds et al., 1987; Schaller et al., 1999). Cells were transfected using lipofectAMINE (Life Technologies) according to the manufacturer's instructions or infected with retroviral stocks (Schaller et al., 1999). Approximately 7–9 days post transfection or 5–7 days post infection, cells were lysed.

Western Blotting

Cells were lysed in Tx-RIPA buffer, and protein concentrations were determined using the bicinchoninic acid assay (Pierce) (Thomas et al., 1999). Equal amounts of lysate (25 μg) were analyzed for FAK expression by Western blotting with the BC4 polyclonal antiserum. Src expression was detected with monoclonal antibody EC10 (Upstate Biotech), and the FAK phosphorisomer specifically phosphorylated on tyrosine 925 was detected with the PY925 antibody (Biosource).

In Vitro Kinase Assay

Src^{527F} was immunoprecipitated from ~1 mg of CE cell lysates using the EC10 monoclonal antibody (Upstate Biotechnology) and incubated on ice for 1 hr. The immune complexes were recovered by incubation with protein A Sepharose beads (Amersham Pharmacia Biotech) for 1 hr at 4°C. Immune complexes were washed twice with lysis buffer, twice with Tris-buffered saline (10 mM Tri-HCl [pH 7.5], 150 mM NaCl) and twice with kinase reaction buffer (20 mM PIPES [pH 7.2], 5 mM $MnCl_2$, 5 mM $MgCl_2$). The immune complexes were then resuspended in kinase reaction buffer containing 35 μM ATP, including 10 μCi of [γ-^{32}P] ATP (6000 Ci/mmol; Perkin Elmer Life Sciences) and incubated with 4 μg of recombinant substrate for various times at room temperature. Reactions were terminated by the addition of sample buffer. Samples were resolved by SDS-PAGE, and the gels were then stained with SYPRO orange (Molecular Probes) according to the manufacturer's instructions. The stained gels were analyzed for fluorescence and by phosphorimaging after drying, using a Molecular Dynamics Storm phosphorimager (Model 860) and ImageQuant software (version 5.2). The ratios of phosphorylation to fluorescence signals of the substrate bands were plotted as a function of time to determine the relative ability of Src^{527F} to phosphorylate each substrate.

Acknowledgments

We would like to thank Alison Worsham for outstanding technical assistance. We would also like to thank Dr. Greg Young and Dr. Ron Venters for their valuable technical assistance in NMR data collection. This project was supported by National Institutes of Health grants GM57943 (M.D.S), DE13079 (M.D.S), and HL45100 (M.D.S. and S.L.C.).

Received: November 17, 2003
Revised: February 3, 2004
Accepted: February 16, 2004
Published: May 11, 2004

References

Arold, S.T., Hoellerer, M.K., and Noble, M.E.M. (2002). The structural basis of localization and signaling by the focal adhesion targeting domain. Structure *10*, 319–327.

Brunger, A.T., Adams, P.D., Clore, G.M., DeLano, W.L., Gros, P., Grosse-Kunstleve, R.W., Jiang, J.S., Kuszewski, J., Nilges, M., Pannu, N.S., et al. (1998). Crystallography & NMR system: a new software suite for macromolecular structure determination. Acta Crystallogr. Biol. Crystallogr. D *54*, 905–921.

Cary, L., Chang, J., and Guan, J. (1996). Stimulation of cell migration

by overexpression of focal adhesion kinase and its association with Src and Fyn. J. Cell Sci. *109*, 1787–1794.

Chen, H.-C., Appeddu, P.A., Parsons, J.T., Hildebrand, J.D., Schaller, M.D., and Guan, J.-L. (1995). Interaction of focal adhesion kinase with cytoskeletal protein talin. J. Biol. Chem. *270*, 16995–16999.

Cooley, M.A., Broome, J.M., Ohngemach, C., Romer, L.H., and Schaller, M.D. (2000). Paxillin binding is not the sole determinant of focal adhesion localization or dominant-negative activity of focal adhesion kinase/focal adhesion kinase-related nonkinase. Mol. Biol. Cell *11*, 3247–3263.

Cornilescu, G., Delaglio, F., and Bax, A. (1999). Protein backbone angle restraints from searching a database for chemical shift and sequence homology. J. Biomol. NMR *13*, 289–302.

Delaglio, F., Grzesiek, S., Vuister, G.W., Zhu, G., Pfeifer, J., and Bax, A. (1995). NMRPipe: a multidimensional spectral processing system based on UNIX pipes. J. Biomol. NMR *6*, 277–293.

Frisch, S.M., Vuori, K., Ruoslahti, E., and Chan-Hui, P.Y. (1996). Control of adhesion-dependent cell survival by focal adhesion kinase. J. Cell Biol. *134*, 793–799.

Gabarra-Niecko, V., Keely, P.J., and Schaller, M.D. (2002). Characterization of an activated mutant of focal adhesion kinase: 'SuperFAK'. Biochem. J. *365*, 591–603.

Gabarra-Niecko, V., Schaller, M.D., and Dunty, J.M. (2003). FAK regulates biological processes important for the pathogenesis of cancer. Cancer Metastasis Rev. *22*, 359–374.

Gao, G., Prutzman, K.C., King, M.L., Scheswohl, D.M., DeRose, E.F., London, R.E., Schaller, M.D., and Campbell, S.L. (2004). NMR solution structure of the focal adhesion targeting domain of focal adhesion kinase in complex with a Paxillin LD peptide: evidence for a two site binding model. J. Biol. Chem. *279*, 8441–8451.

Grzesiek, S., and Bax, A. (1992). Correlating backbone amide and side chain resonances in larger proteins by multiple relayed triple resonance nmr. J. Am. Chem. Soc. *114*, 6291–6293.

Grzesiek, S., Anglister, J., and Bax, A. (1993). Correlation of backbone amide and aliphatic side-chain resonances in 13C/15N-enriched proteins by isotropic mixing of 13C magnetization. J. Magn. Reson. Series B *101*, 114–119.

Hayashi, I., Vuori, K., and Liddington, R.C. (2002). The focal adhesion targeting (FAT) region of focal adhesion kinase is a four-helix bundle that binds paxillin. Nat. Struct. Biol. *9*, 101–106.

Hildebrand, J.D., Schaller, M.D., and Parsons, J.T. (1993). Identification of sequences required for the efficient localization of the focal adhesion kinase, pp125FAK, to cellular focal adhesions. J. Cell Biol. *123*, 993–1005.

Hildebrand, J., Schaller, M., and Parsons, J. (1995). Paxillin, a tyrosine phosphorylated focal adhesion-associated protein binds to the carboxyl terminal domain of focal adhesion kinase. Mol. Biol. Cell *6*, 637–647.

Hoellerer, M.K., Noble, M.E.M., Labesse, G., Campbell, I.D., Werner, J.M., and Arold, S.T. (2003). Molecular recognition of paxillin LD motifs by the focal adhesion targeting domain. Structure *11*, 1207–1217.

Hubbard, S.R. (1997). Crystal structure of the activated insulin receptor tyrosine kinase in complex with peptide substrate and ATP analog. EMBO J. *16*, 5572–5581.

Hungerford, J.E., Compton, M.T., Matter, M.L., Hoffstrom, B.G., and Otey, C.A. (1996). Inhibition of pp125FAK in cultured fibroblasts results in apoptosis. J. Cell Biol. *135*, 1383–1390.

Ikura, M., Kay, L.E., and Bax, A. (1990). A novel approach for sequential assignment of 1H, 13C, and 15N spectra of proteins: heteronuclear triple-resonance three-dimensional NMR spectroscopy. Biochemistry *29*, 4659–4667.

Ikura, M., Kay, L.E., and Bax, A. (1991). Improved three-dimensional 1H–13C–1H correlation spectroscopy of a 13C-labeled protein using constant-time evolution. J. Biomol. NMR *1*, 299–304.

Ilic, D., Furuta, Y., Kanazawa, S., Takeda, N., Sobue, K., Nakatsuji, N., Nomura, S., Fujimoto, J., Okada, M., and Yamazaki, T. (1995). Reduced cell motility and enhanced focal adhesion contact formation in cells from FAK-deficient mice. Nature *377*, 539–544.

Johnson, B., and Blevins, R.A. (1994). NMRView: a computer program for the visualization and analysis of NMR data. J. Biomol. NMR *4*, 603–614.

Katz, B.-Z., Romer, L., Miyamoto, S., Volberg, T., Matsumoto, K., Cukierman, E., Gieger, B., and Yamada, K.M. (2003). Targeting membrane-localized FAK to focal adhesions: roles of tyrosine phosphorylation and Src family kinases. J. Biol. Chem. *287*, 29115–29120. Published online May 16, 2003. 10.1074/jbc.M212396200.

Kay, L.E., Keifer, P., and Saarinsen, T. (1992). Pure absorption gradient enhanced heteronuclear single quantum correlation spectroscopy with improved sensitivity. J. Am. Chem. Soc. *114*, 10663–10665.

Kay, L.E., Xu, X., and Yamazaki, T. (1994). Enhanced-sensitivity triple-resonance spectroscopy with minimal H2O saturation. J. Magn. Reson. Series A *109*, 129–133.

Koradi, R., Billeter, M., and Wüthrich, K. (1996). MOLMOL: a program for display and analysis of macromolecular structures. J. Mol. Graph. *14*, 51–55.

Laskowski, R.A., Rullmannn, J.A., MacArthur, M.W., Kaptein, R., and Thornton, J.M. (1996). AQUA and PROCHECK-NMR: programs for checking the quality of protein structures solved by NMR. J. Biomol. NMR *8*, 477–486.

Lin, T.H., Aplin, A.E., Shen, Y., Chen, Q., Schaller, M., Romer, L., Aukhil, I., and Juliano, R.L. (1997). Integrin-mediated activation of MAP kinase is independent of FAK: evidence for dual integrin signaling pathways in fibroblasts. J. Cell Biol. *136*, 1385–1395.

Linge, J.P., and Nilges, M. (1999). Influence of non-bonded parameters on the quality of NMR structures: a new force field for NMR structure calculation. J. Biomol. NMR *13*, 51–59.

Liu, G., Guibao, C.D., and Zheng, J. (2002). Structural insight into the mechanisms of targeting and signaling of focal adhesion kinase. Mol. Cell. Biol. *22*, 2751–2760.

Matsuo, H., Kupce, E., Li, H., and Wagner, G. (1996). Increased sensitivity in HNCA and HN(CO)CA experiments by selective C beta decoupling. J. Magn Reson. Series B *113*, 91–96.

McIntosh, L.P., and Dahlquist, F.W. (1990). Biosynthetic incorporation of 15N and 13C for assignment and interpretation of nuclear magnetic resonance spectra of proteins. Q. Rev. Biophys. *23*, 1–38.

Nilges, M. (1995). Calculation of protein structures with ambiguous distance restraints. Automated Assignment of ambiguous NOE crosspeaks and disulphide connectivities. J. Mol. Biol. *245*, 645–660.

Nilges, M. (1997). Ambiguous distance data in the calculation of NMR structures. Fold. Des. *2*, s53–s57.

Odaert, B., Landrieu, I., Dijkstra, K., Schuurman-Wolters, G., Casteels, P., Wieruszeski, J.-M., Inze, D., Scheek, R., and Lippens, G. (2002). Solution NMR study of the monomeric form of p13suc1 protein sheds light on the hinge region determining the affinity for a phosphorylated substrate. J. Biol. Chem. *277*, 12375–12381.

Ottiger, M., Delaglio, F., and Bax, A. (1998). Measurement of J and dipolar couplings from simplified two-dimensional NMR spectra. J. Magn. Reson. *131*, 373–378.

Parsons, J.T. (2003). Focal adhesion kinase: the first ten years. J. Cell Sci. *116*, 1409–1416.

Pascal, S.M., Muhandiram, D.R., Yamazaki, T., Forman-Kay, J.D., and Kay, L.E. (1994). Simultaneous acquisition of 15N and 13C NOE spectra of proteins in H2O. J. Magn. Reson. Series B *103*, 197–201.

Rahuel, J., Gay, B., Erdmann, D., Strauss, A., Garcia-Echeverria, C., Furet, P., Caravatti, G., Fretz, H., Schoepfer, J., and Grutter, M. (1996). Structural basis for specificity of Grb2–SH2 revealed by a novel ligand binding mode. Nat. Struct. Biol. *3*, 586–589.

Reynolds, A.B., Vila, J., Lansing, T.J., Potts, W.M., Weber, M.J., and Parsons, J.T. (1987). Activation of the oncogenic potential of the avian cellular src protein by specific structural alteration of the carboxy terminus. EMBO J. *6*, 2359–2364.

Reynolds, A.B., Roesel, D.J., Kanner, S.B., and Parsons, J.T. (1989). Transformation-specific tyrosine phosphorylation of a novel cellular

protein in chicken cells expressing oncogenic variants of the avian cellular src gene. Mol. Cell. Biol. *9*, 629–638.

Rousseau, F., Schymkowitz, J.W.H., Wilkinson, H.R., and Itzhaki, L.S. (2001). Three-dimensional domain swapping in p13suc1 occurs in the unfolded state and is controlled by conserved proline residues. Proc. Natl. Acad. Sci. USA *98*, 5596–5601.

Schaller, M.D. (2001). Biochemical signals and biological responses elicited by the focal adhesion kinase. Biochim. Biophys. Acta *1540*, 1–21.

Schaller, M.D., Hildebrand, J.D., and Parsons, J.T. (1999). Complex formation with focal adhesion kinase: a mechanism to regulate activity and subcellular localization of Src kinases. Mol. Biol. Cell *10*, 3489–3505.

Schlaepfer, D.D., and Hunter, T. (1996). Evidence for in vivo phosphorylation of the Grb2 SH2-domain binding site on focal adhesion kinase by Src-family protein-tyrosine kinases. Mol. Cell. Biol. *16*, 5623–5633.

Schlaepfer, D.D., and Hunter, T. (1997). Focal adhesion kinase overexpression enhances Ras-dependent integrin signaling to ERK2/mitogen-activated protein kinase through interactions with and activation of c-Src. J. Biol. Chem. *272*, 13189–13195.

Schlaepfer, D.D., Hanks, S.K., Hunter, T., and van der Geer, P. (1994). Integrin-mediated signal transduction linked to Ras pathway by GRB2 binding to focal adhesion kinase. Nature *372*, 786–791.

Schlaepfer, D.D., Hauck, C.R., and Sieg, D.J. (1999). Signaling through focal adhesion kinase. Prog. Biophys. Mol. Biol. *71*, 435–478.

Tachibana, K., Sato, T., D'Avirro, N., and Morimoto, C. (1995). Direct association of pp125FAK with paxillin, the focal adhesion-targeting mechanism of pp125FAK. J. Exp. Med. *182*, 1089–1099.

Thomas, J.W., Ellis, B., Boerner, R.J., Knight, W.B., White, G.C., II, and Schaller, M.D. (1998). SH2- and SH3-mediated interactions between focal adhesion kinase and Src. J. Biol. Chem. *273*, 577–583.

Thomas, J.W., Cooley, M.A., Broome, J.M., Salgia, R., Griffin, J.D., Lombardo, C.R., and Schaller, M.D. (1999). The role of focal adhesion kinase binding in the regulation of tyrosine phosphorylation of paxillin. J. Biol. Chem. *274*, 36684–36692.

Wary, K.K., Mainiero, F., Isakoff, S.J., Marcantonio, E.E., and Giancotti, F.G. (1996). The adapter protein Shc couples a class of integrins to the control of cell cycle progression. Cell *87*, 733–743.

Wittekind, M., and Mueller, L. (1993). HNCACB, a high-sensitivity 3D NMR experiment to correlate amide-proton and nitrogen resonances with the alpha- and beta-resonances in proteins. J. Magn. Reson. Series B *101*, 201–205.

Xu, L.H., Yang, X., Craven, R.J., and Cance, W.G. (1998). The COOH-terminal domain of the focal adhesion kinase induces loss of adhesion and cell death in human tumor cells. Cell Growth Differ. *9*, 999–1005.

Yamazaki, T., Forman-Kay, J.D., and Kay, L.E. (1993). Two-dimensional NMR experiments for correlating carbon-13.beta., and proton.delta./.epsilon. chemical shifts of aromatic residues in 13C-labeled proteins via scalar couplings. J. Am. Chem. Soc. *115*, 11054–11055.

Yang, D., Tolman, J.R., Goto, N.K., and Kay, L.E. (1998). An HNCO-based pulse scheme for the measurement of 13Ca-1Ha one-bond dipolar couplings in 15N, 13C labeled proteins. J. Biomol. NMR *12*, 325–332.

Yang, D., Venters, R.A., Mueller, G.A., Choy, W.Y., and Kay, L.E. (1999). TROSY-based HNCO pulse sequences for the measurement of 1HN-15N, 15N–13CO, 1HN-13CO, 13CO-13CA, and 1HN-13CA dipolar couplings in 15N, 13C, 2H labeled proteins. J. Biomol. NMR *14*, 333–343.

Zheng, C., Xing, Z., Bian, Z.C., Guo, C., Akbay, A., Warner, L., and Guan, J.-L. (1998). Differential regulation of Pyk2 and focal adhesion kinase (FAK). The C-terminal domain of FAK confers response to cell adhesion. J. Biol. Chem. *273*, 2384–2389.

Accession Numbers

The 20 lowest energy structures of the avian FAT domain have been submitted to the PDB under code number 1PV3.